Butyrate oxidation attenuates the butyrate-induced improvement of insulin sensitivity in myotubes

Rios-Morales, Melany; Vieira-Lara, Marcel A.; Homan, Esther; Langelaar-Makkinje, Miriam; Gerding, Albert; Li, Zhuang; Huijkman, Nicolette; Rensen, Patrick C. N.; Wolters, Justina C.; Reijngoud, Dirk-Jan

Published in:
Biochimica et biophysica acta-Molecular basis of disease

DOI:
10.1016/j.bbadis.2022.166476

Publication date:
2022

BBA - Molecular Basis of Disease 1868 (2022) 166476

Contents lists available at ScienceDirect

BBA - Molecular Basis of Disease

journal homepage: www.elsevier.com/locate/bbadis

Butyrate oxidation attenuates the butyrate-induced improvement of insulin sensitivity in myotubes

Melany Rios-Morales [a,1], Marcel A. Vieira-Lara [a,1], Esther Homan [a], Miriam Langelaar-Makkinje [a], Albert Gerding [a,b], Zhuang Li [c,d], Nicolette Huijkman [a], Patrick C.N. Rensen [c,d], Justina C. Wolters [a], Dirk-Jan Reijngoud [a], Barbara M. Bakker [a,*]

[a] Laboratory of Pediatrics, Center for Liver, Digestive, and Metabolic Diseases, University of Groningen, University Medical Center Groningen, the Netherlands
[b] Department of Laboratory Medicine, University of Groningen, University Medical Center Groningen, Groningen, the Netherlands
[c] Department of Medicine, Division of Endocrinology, Leiden University Medical Center, Leiden, the Netherlands
[d] Einthoven Laboratory for Experimental Vascular Medicine, Leiden University Medical Center, Leiden, the Netherlands

ARTICLE INFO

Keywords:
Butyrate
Skeletal muscle
Insulin resistance
Fatty-acid oxidation
Glycolysis

ABSTRACT

Skeletal muscle insulin resistance is a key pathophysiological process that precedes the development of type 2 diabetes. Whereas an overload of long-chain fatty acids can induce muscle insulin resistance, butyrate, a short-chain fatty acid (SCFA) produced from dietary fibre fermentation, prevents it. This preventive role of butyrate has been attributed to histone deacetylase (HDAC)-mediated transcription regulation and activation of mitochondrial fatty-acid oxidation. Here we address the interplay between butyrate and the long-chain fatty acid palmitate and investigate how transcription, signalling and metabolism are integrated to result in the butyrate-induced skeletal muscle metabolism remodelling. Butyrate enhanced insulin sensitivity in palmitate-treated, insulin-resistant C2C12 cells, as shown by elevated insulin receptor 1 (IRS1) and pAKT protein levels and *Slc2a4* (GLUT4) mRNA, which led to a higher glycolytic capacity. Long-chain fatty-acid oxidation capacity and other functional respiration parameters were not affected. Butyrate did upregulate mitochondrial proteins involved in its own oxidation, as well as concentrations of butyrylcarnitine and hydroxybutyrylcarnitine. By knocking down the gene encoding medium-chain 3-ketoacyl-CoA thiolase (MCKAT, *Acaa2*), butyrate oxidation was inhibited, which amplified the effects of the SCFA on insulin sensitivity and glycolysis. This response was associated with enhanced HDAC inhibition, based on histone 3 acetylation levels. Butyrate enhances insulin sensitivity and induces glycolysis, without the requirement of upregulated long-chain fatty acid oxidation. Butyrate catabolism functions as an escape valve that attenuates HDAC inhibition. Thus, inhibition of butyrate oxidation indirectly prevents insulin resistance and stimulates glycolytic flux in myotubes treated with butyrate, most likely via an HDAC-dependent mechanism.

1. Introduction

Skeletal muscle is a major site of insulin-stimulated glucose uptake and therefore plays a critical role in glucose homeostasis. In an obese condition, an overload of lipids may induce the tissue to become insulin resistant, a pathophysiological process that precedes the development of type 2 diabetes [1]. This has been mechanistically linked to increased content of complex lipid species, such as ceramides and diacylglycerols. These lipids inhibit components of the insulin signalling cascade, namely insulin receptor substrate (IRS) and protein kinase B (AKT), which leads to less translocation of GLUT4 to the plasma membrane and thereby decreases glucose uptake [2]. Long-chain fatty acids such as palmitate (C16:0) and oleate (C18:1), are activated by cytosolic acyl-CoA synthetases (ACS) to form long-chain acyl-CoA [3]. These are converted to acylcarnitines by carnitine palmitoyltransferase 1 (CPT1) and enter the mitochondria to be oxidized in the β-oxidation pathway [4]. Higher clearance of long-chain fatty-acids by increased mitochondrial oxidative capacity has been related to decreased accumulation of complex lipids and consequently improved insulin sensitivity [5,6].

In contrast to long-chain fatty acids, short-chain fatty acids (SCFA)

* Corresponding author.
E-mail address: b.m.bakker01@umcg.nl (B.M. Bakker).
[1] These authors contributed equally.

https://doi.org/10.1016/j.bbadis.2022.166476
Received 4 February 2022; Received in revised form 31 May 2022; Accepted 25 June 2022
Available online 8 July 2022

can enhance insulin sensitivity. These SCFA, mainly acetate, propionate and butyrate, are the most abundant products of dietary fibre fermentation by the gut microbiota in the colon [7]. Locally, they can induce the production of the satiety hormones glucagon-like peptide-1 and peptide YY by enteroendocrine cells and reduce inflammation by affecting the local immune system. Alternatively, SCFA are taken up and metabolized by the host [8]. Rodent experiments with isotopically labelled SCFA demonstrated that their absorption rate, but not their caecal concentration, correlates with metabolic health, suggesting that they exert their effects at least partially when taken up by the host [9]. High-fibre diets are known to exert a series of beneficial systemic effects, including prevention and treatment of metabolic syndrome, an effect that is mimicked by administration of SCFA [7,10].

Butyrate enhanced insulin sensitivity when exogenously administered to mice as measured by hyperinsulinemic-euglycemic clamps and insulin tolerance tests [11,12]. Likewise, an increase of butyrate-producing bacteria in the intestine correlated with improved insulin sensitivity in human subjects with metabolic syndrome [13]. These beneficial effects of butyrate on systemic insulin response have been linked to a remodelling in various tissues. Among such effects, decreased adipose tissue lipolysis preventing the excess of lipid supply to other tissues [14–16], and increased lipid oxidation in liver [11] have been reported. In addition, butyrate can modulate insulin secretion through GPR receptor signalling in pancreatic β-cells [17,18]. Recent data show that butyrate can improve metabolic health by vagal activation [19]. Skeletal muscle insulin sensitivity has also been shown to improve after butyrate treatment [12]. However, whether this relates to a direct effect of the SCFA on the tissue or as a consequence of interorgan crosstalk is not yet fully elucidated.

Butyrate enters skeletal muscle cells via the highly abundant monocarboxylate transporters MCT-1 and MCT-4 [20] where it may exert multiple effects. First, butyrate acts as regulator of gene expression via competitive inhibition of histone deacetylases (HDAC) [21,22]. HDAC inhibition increases transcription of target genes involved in muscle glucose metabolism [23] and insulin signalling [24,25]. Second, butyrate has been shown to enhance mitochondrial biogenesis and fatty acid oxidation in the skeletal muscle both in vivo [12,26,27] and in vitro [12,28]. Last, but not least, butyrate itself may also be oxidized in the mitochondria [29]. However, the range of experimental conditions (in vivo versus in vitro, different diets and culturing conditions) makes it difficult to address how these different effects of butyrate interact and consequently affect insulin sensitivity.

Here we investigate the interplay between butyrate-induced (i) remodelling of mitochondrial metabolism and (ii) transcription regulation, and their effect on insulin sensitivity. To address this, we took a systemic approach to dissect the direct effects of butyrate on metabolic and signalling pathways at the level of genes, proteins and function, in insulin-sensitive (control) and insulin-resistant C2C12 cells.

2. Materials and methods

2.1. Cell culture

The C2C12 mouse myoblast cell line (C2C12) was obtained from ATCC. Myoblasts were cultured at 37 °C and 5 % CO_2 in DMEM (P04-01500; PAN Biotech), supplemented with 11 mM glucose, 10 % Fetal Bovine Serum (FBS, Gibco 10270106) and 4 mM glutamine (Gln). Cells were passaged every other day. To induce differentiation into myotubes, cells were plated 10,000–15,000 cells/cm^2. After 2 days, the medium was replaced by differentiation medium, which contained 2 % horse serum (Sigma H1270) instead of FBS and was otherwise identical to the culture medium. Differentiation medium was refreshed every other day. After 4 days of differentiation, cells were incubated for 24 h in minimal DMEM (5.5 mM glucose) supplemented with 4 mM Gln, 0.5 % BSA or 500 μM BSA-conjugated palmitate were added, together with 2 mM L-carnitine and 3 mM sodium butyrate (Buty) or 3 mM sodium chloride as control (Ctrl). A stock solution was prepared of 10 mM palmitate conjugated to BSA as follows. Palmitate (Sigma P9767) was dissolved in 100 % ethanol in a glass tube. The solution was incubated at 50 °C and alternately sonicated (VWR USC THD Ultrasound water sonicator, power 9, 5 min cycles) and vortexed, until it became opaque. Samples were subsequently dried at 70 °C under N_2 stream. In parallel, a 10 % solution of fatty-acid-free BSA solution was prepared in PBS and added to the dried palmitate to obtain a final concentration of 10 mM palmitate. The solution was incubated at 37 °C alternating vortexing with sonication until a translucent solution was obtained and pH was adjusted to 7.0 (NaOH). Viability of differentiated C2C12 myotubes was measured in 96-wells plates with the use of alamarBlue™ HS Cell Viability Reagent (Invitrogen A50100) according to the manufacturer's instructions.

2.2. Animals

Male APOE*3-Leiden.CETP (E3L.CETP) mice, a well-established model of human-like lipid metabolism, were obtained as previously described [30] and housed under standard conditions in conventional cages with ad libitum access to regular chow diet and water unless indicated otherwise. 12–14 weeks old mice received a high-fat diet (HFD) (60 % kcal derived from lard fat and 0.25 % cholesterol (w/w), Research Diets, New Brunswick, NJ) without (control group; $n = 6$) or with 5 % (w/w) sodium butyrate (Sigma Aldrich; butyrate group; $n = 8$) for 6 weeks. Quadriceps tissue was isolated and homogenized in NP-40 buffer (7.5 % w/v) as described in Vieira-Lara et al. [31]. These samples were used for Western Blots, as described in Section 2.5. All animal experiments were performed under approval by the Ethics Committee on Animal Care and Experimentation of the Leiden University Medical Center and following the regulations of the Dutch law on animal welfare.

2.3. Transfection and viral transduction

Lentiviral production was achieved through transient transfection of HEK293T cells with packaging and expression lentiviral vectors and a pLKO.1 plasmid with the gene of interest and polyethylenimine (Polysciences 23966-2). The shRNA target sequences were: GACTTCTCTGCCACCGATTTA for *Acaa2* knockdown, CAGAATGCCTTCAAGGTATTT for *Pfkfb2* knockdown, and empty pLKO.1 vector as control. Culture supernatants containing viral particles were harvested 48 h later, and after filtration through a 0.45-μm filter, this supernatant was applied to undifferentiated C2C12 cells seeded 24 h before ($0.4 \bullet 10^5$ cells/well, 6-well plate). The lentiviral expression vectors used here included puromycin resistance as selection marker to select stably transduced polyclonal cells. Puromycin was used at a concentration of 2 μg/mL and removed prior to cell differentiation and subsequent experimental incubations.

2.4. RNA isolation and qRT-PCR

RNA isolation was done with the RNeasy mini kit (Qiagen 74106) following the manufacturer's protocol. RNA was reverse transcribed with M-MLV Reverse Transcriptase, RNase H Minus (Promega). For quantitative PCR, cDNA was amplified using SYBR Green Mixture (Bio-rad Laboratories) in a real-time polymerase chain reaction cycler (QuantStudio 7 Flex Real-Time PCR System, Applied Biosystems) and data were analysed using QuantStudio™ Real-Time PCR Software (v1.2). Primers can be found in Table 1. Throughout the text, gene names start with a capital letter and are written in italic, and 'mRNA levels' is stated when it concerns qPCR data.

2.5. Western blots

After incubation with butyrate for 24 h, the medium was removed and minimal DMEM was added in the presence of 100 nM insulin (Sigma

Table 1
List of oligonucleotide primer pairs used in qPCR analysis.

Gene	Forward (5′-3′)	Reverse (5′-3′)
Acaa2	CTGCTACGAGGTGTGTTCATC	AGCTCTGCATGACATTGCCC
Acadm	GCTAGTGGAGCACCAAGGAG	CCAGGCTGCTCTCTGGTAAC
Ckm	CTGACCCCTGACCTCTACAAT	CATGGCGGTCCTGGATGAT
Cpt1b	GCACACCAGGCAGTAGCTTT	CAGGAGTTGATTCCAGACAGGTA
Crat	GCTGCCAGAACCGTGGTAAA	CCTTGAGGTAATAGTCCAGGGA
Gapdh	ATTGTCAGCAATGCATCCTG	ATGGACTGTGGTCATGAGCC
Myod1	CCACTCCGGGACATAGACTTG	AAAAGCGCAGGTCTGGTGAG
Myog	GAGACATCCCCCTATTTCTACCA	GCTCAGTCCGCTCATAGCC
Pfkfb2	GACAAGCCAACTCACAACTTCC	ACACTGTAATTTCTTGGACGCC
Slc16a1	TGTTAGTCGGAGCCTTCATTTC	CACTGGTCGTTGCACTGAATA
Slc2a1	TTCTCTGTCGGCCTCTTTGT	GAGAAGCCCATAAGCACAGC
Slc2a4	GCCCGGACCCTATACCCTAT	AGTGTTCCAGTCACTCGCTG

I1882) for the indicated time. Subsequently, cells were washed twice with PBS, and RIPA buffer (DPBS, Gibco 14190 supplemented with 1 % v/v NP-40, 5 g/L sodium deoxycholate and 1 g/L SDS) was added to the cells in the presence of cOmplete protease inhibitor cocktail (1:25, Merck 11836145001) and phosphatase inhibitor cocktail 2 and 3 (1:100 each, Sigma P5726, P0044). Cells were scraped, centrifuged at 6000*g* for 10 min and the pellet was discarded. Protein content was normalized with the Pierce BCA Protein Assay Kit (ThermoFisher 23225). Afterwards, SDS loading buffer was added to samples, which were stored at −80 °C until analysis. Prior to loading, samples were heated at 95 °C for 5 min. In total 10–20 μg protein was loaded for each cell extract and 24 μg for mouse quadriceps homogenates. The subsequent protocol was adapted from [32]. Briefly, proteins were separated in 8 to 12 % acrylamide gels in running buffer (0.2 M glycine, 25 mM Tris and 0.1 % SDS) with a MiniPROTEAN Tetra Vertical Electrophoresis Cell system (Cat. No. 1658029FC; Bio-Rad) with the voltage ranging from 90 to 150 V. Polyvinylidene difluoride (PVDF) membranes were used for transfer, performed in blotting buffer (0.1 M glycine, 50 mM Tris, 0.01 % SDS and 10 % methanol, pH 8.3) at 45 V for 1 h 45 min. Blocking was performed in 5 % BSA in TBST for 1 h and primary antibodies were incubated overnight at 4 °C.

Subsequently, TBST wash was performed 3 times followed by incubation with HRP-coupled secondary antibody (goat anti-mouse or goat anti-rabbit) for 2 h. TBST wash was performed 3 times before detection. Pierce ECL substrate (Thermo Fisher Scientific, 32209) was used for detection using Image Quant LAS4000 Mini (GE Healthcare) (11). Pixel quantification from single lanes were normalized to the average of all lanes before normalization to the respective protein loading control. The choice of the loading control was based on the size of the protein to achieve a good separation with the protein of interest. Throughout the text, protein levels are denoted by capital letters according to the guidelines of nomenclature for mouse proteins. All representatives images of western blot data included in the main text are depicted in Supplemental Data 1.

Antibodies used: actin (Millipore MAB1501, 1:10,0000), ACC (Cell Signaling, 3676, 1:1000), pACC(S79) (Cell Signaling, 3661, 1:2000), MCD (Abcam, ab95945, 1:1000), GAPDH (Abcam, ab37187, 1:20,000), PGC1α (Abcam, ab54481, 1:1000), IRS1 (Cell Signaling 2328), pIRS1 (S636/639) (Cell Signaling 2388), AKT (Cell Signaling 4691), pAKT (T308) (Cell Signaling 2965), pAKT (S473) (Cell Signaling 4060), CD36 (developed in the lab of Prof Dr. Huy Ong [33] and provided as a kind gift from Prof. Debby Koonen), ACAA2 (MCKAT) (Abcam ab237540), PFKFB2 (Cell Signaling 13029), HSP90 (Cell Signaling 4874), PDK4 (Abcam ab214938) and secondary antibodies anti-rabbit (Thermo Fisher 31460) and anti-mouse (Thermo Fisher 31430).

2.6. Quantitative targeted proteomics

Quantitative targeted proteomics was performed according to Wolters et al. [34] and adapted according to Vieira-Lara et al. [31]. After 24 h incubation with butyrate, cells were washed once with PBS and harvested in lysis buffer (0.1 % v/v NP-40, 0.4 M NaCl, 10 mM Tris–HCl and 1 mM EDTA, pH 8.0) supplemented with cOmplete protease inhibitor cocktail (1:25). Samples were incubated at 4 °C in a Rotator (Stuart SB3) at 40 rpm for 15 min. While kept on ice, samples were sonicated at 30 % amplitude 10 s on/5 s off for 5 cycles (Ultrasonic Processor VCX 130, Sonics & Materials, Inc). Subsequently, samples were centrifuged at 12,000*g* for 10 min, the supernatants were collected and protein content was determined as mentioned in Section 2.4. Isotopically-labelled concatemer derived standard peptides have been previously selected for targets of interest (QconCAT technology, PolyQuant GmbH Germany). In-gel digestion of proteins and QconCATs, LC-MS and data analysis have been performed as previously described. Sequences of ^{13}C-labelled peptide standards are found in Appendix 1.

2.7. Acylcarnitine profiling

Acylcarnitine profiles were obtained as described by Derks et al. with slight modifications [35]. After 24 h incubation with butyrate, medium was collected, cells were washed once with PBS and harvested in PBS supplemented with cOmplete protease inhibitor cocktail (1:25). 10 μL of either cell suspension or medium were collected per sample, followed by the addition of 100 μL of acetonitrile and 100 μL of internal standard (L-carnitine-[D_3], acetyl-L-carnitine-[D_3], propionyl-L-carnitine-[D_3], octanoyl-L-carnitine-[D_3], and palmitoyl-L-carnitine-[D_3]). Samples were then centrifuged at 20,000*g* for 10 min, collected into glass vials and analysed by LC-MS/MS with the use of an API 4500 triple quadrupole mass spectrometer and selected ion monitoring as previously described.

2.8. Triglycerides

Cells were collected in 500 μL TBS buffer on ice after stimulation. While kept on ice, samples were sonicated at 30 % amplitude for 2 s (Ultrasonic Processor VCX 130, Sonics & Materials, Inc). Protein content was adjusted with the Pierce BCA Protein Assay Kit (ThermoFisher 23,225). Fat was extracted using a modification of the Bligh & Dyer method [36]. In short, 400 μL of sample was mixed with 1500 μL of chloroform: methanol (2:1) in a glass tube, and vortexed for 30 min at 4 °C. Subsequently, 600 μL of miliQ water and 500 μL of chloroform were added, and mixtures were vortexed for 5 min and subsequently centrifuged at 1500*g* for 10 min. From the lower chloroform layer, 900 μL was transferred to a new glass tube and dried under N_2 stream. Lipids were dissolved in 150 μL of 2 % triton-X in chloroform, dried under N_2 and dissolved in 150 μL miliQ water while shaking at 37 °C in a water bath. Triglyceride content was determined using a Trig/GB kit (Roche Molecular Biochemicals, 11877771) according to the protocol provided by the manufacturer.

2.9. Extracellular acidification rate (ECAR) and cellular oxygen consumption rate (OCR)

2000 cells were seeded per well in a 96 wells Seahorse plate (V3-PS 101085), kept in growth medium for 2 days and changed to differentiation medium for 4 days. After 24 h incubation with butyrate or Ctrl (as described in Section 2.1.), cells were washed twice and kept in KHB solution (11 mM NaCl, 4.7 mM KCl, 2 mM $MgSO_4$, 1.25 mM $CaCl_2$ and 1.2 mM NaH_2PO_4 supplemented with 0.5 mM carnitine and 2.5 mM glucose) at pH 7.4. To determine glucose-based respiration, modified KHB was used with glucose supplemented to 10 mM final concentration and in the presence of 2 mM of glutamine. Insulin (100 nM) was added where indicated and incubated for 30 min before loading the plate into the Seahorse Xfe flux analyzer (Agilent, Santa Clara, United States). For palmitate-based respiration, cells were incubated in KHB solution with 500 μM palmitate (conjugated with 0.5 % BSA) or 0.5 % BSA and incubated for 30 min before loading the plate into the Seahorse Xfe flux analyzer. During the assay, indicated inhibitors and uncoupler were

added at the following concentration: for ECAR measurements, oligomycin (2.5 μM) and bromopyruvate (100 μM), for OCR measurements oligomycin (2.5 μM), dinitrophenol (50 μM) and rotenone (2 μM) and antimycin (4 μM). To normalize the results by protein content, cells were immediately lysed after the end of the measurements. Briefly, all remaining medium was removed from the wells and 40 μL of RIPA buffer was added per well. Protein content was determined using the Pierce BCA Protein Assay Kit (Thermo Fisher 23225). Seahorse data was exported with the use of Wave Desktop (Agilent Biosciences) and calculations were performed according to manufacturer's instructions.

2.10. Mitochondrial oxygen consumption in permeabilized cells by high resolution respirometry

Mitochondrial oxygen consumption rates were measured in a two-channel high-resolution Oroboros oxygraph-2k (Oroboros, Innsbruck, Austria) in permeabilized cells (0.02 mg/mL digitonin). After 24 h incubation with butyrate or Ctrl, cells were washed 1× with PBS, and subsequently 1 mL of trypsin (Gibco 25200056) was added. After 5 min at 37 °C, cells were washed twice with 9 mL of ice-cold PBS and centrifuged at 600*g* for 1 min. The pellet was resuspended in 5 mL Mir05 buffer (respiration buffer) containing 110 mM sucrose, 60 mM potassium lactobionate, 20 mM taurine, 20 mM HEPES, 0.5 mM EGTA, 10 mM KH_2PO_4, 3 mM $MgCl_2$, 1 mg/mL BSA at pH 7.1 at 37 °C [37]. Different substrate combinations were used: (i) 25 μM palmitoyl-CoA and 2 mM L-carnitine, (ii) 25 μM palmitoylcarnitine, or (iii) 2 mM pyruvate, each in the presence of 2 mM malate. ADP-stimulated respiration (state 3) was measured in the presence of 1 mM ADP. State 4 rates were measured after addition of 2 μg/mL of oligomycin. All data was normalized for protein content as determined with the Pierce BCA Protein Assay Kit (ThermoFisher 23225).

2.11. Statistical analysis

Data visualization and analysis were performed with GraphPad Software Inc., version 9.1, 2020. Data are shown as mean ± SEM unless otherwise stated and analyses were conducted with unpaired *t*-tests comparing two means. When the effect of butyrate and palmitate were simultaneously addressed, two-way ANOVA tests were used. When the additional effect of genotype was considered, three-way ANOVA tests were performed. Šidák multiple comparison tests were performed to compare individual means.

3. Results

3.1. Butyrate alleviates palmitate-induced insulin resistance in C2C12 skeletal muscle cells

Long-chain fatty acids inhibit insulin signalling in the skeletal muscle [1]. Insulin binds to the insulin receptor and recruits IRS1, which is thereby activated via the phosphorylation of tyrosine residues. This will lead to the phosphorylation of AKT at residues T308 and S473, a representative readout for insulin sensitivity, and to subsequent translocation of GLUT4 to the plasma membrane [38] (Fig. 1A). When C2C12 myotubes were stimulated with insulin, AKT phosphorylation at T308 and S473 increased without affecting total AKT levels. Phosphorylation at both T308 and S473 was significantly reduced by a 24 h pre-incubation with palmitate (Fig. 1B, S1A). Concomitantly, lactate production in palmitate-treated cells was lower than in controls, indicating a reduction of the glycolytic flux (Fig. S1B). Together, this validated the palmitate-induced, insulin-resistant phenotype in differentiated C2C12 cells.

To examine the effect of butyrate on insulin sensitivity, palmitate-treated and control myotubes were incubated with butyrate for 24 h. Butyrate did not affect cell viability (Fig. S1C). In agreement with previous findings in L6 myotubes [24], butyrate significantly increased IRS1 protein levels in control and palmitate-treated cells, irrespective of insulin stimulation (Fig. 1C–E). Total AKT levels remained approximately constant during insulin stimulation and were barely affected by butyrate (Fig. 1C, F–G). Butyrate stimulated the initial rate and maximum level of AKT phosphorylation in both groups, but mostly in the palmitate group (Fig. 1C, J–K). As a consequence of higher pAKT, which induces a feedback loop (Fig. 1A), butyrate-treated cells had also higher levels of pIRS1(S636/639) (Fig. 1C, H–I). Phosphorylation of IRS1 at S636/639 targets the receptor for degradation (Fig. 1A). Due to this negative feedback loop, total IRS1 levels decreased over time (Fig. 1C, D–E). However, on average, the levels of total IRS1 protein, the result of the balance between IRS synthesis and degradation, remained higher during the time course in the butyrate group (Fig. 1C–E).

It is worth mentioning, that the ratio of phosphorylated to total respective protein gives insight in the activity of the upstream phosphorylation cascade. However, the downstream effect of the phosphorylated proteins on metabolism, which is the focus of this study, depends on the total amount of phosphorylated protein. For this reason, phosphorylated protein concentrations were normalized to loading controls, as indicated in the figure legends and graph axes. Plotting pIRS1 vs IRS1 would lead to an apparent decrease in IRS1 phosphorylation in the butyrate group, given the difference in IRS1 levels among groups (Fig. S1D–E). A similar reasoning applies to pAKT/AKT, in which the effect of butyrate on palmitate is reduced after 15 min (Fig. S1F–G). Altogether, these results demonstrate that butyrate increases the insulin signalling response in both healthy and palmitate-treated myotubes, but to a higher extent in the latter.

3.2. Butyrate is actively metabolized by myotubes, but does not enhance long-chain fatty-acid oxidation

Butyrate was shown to enhance long-chain fatty-acid oxidation capacity in the skeletal muscle [12], which could contribute to the systemic increase in insulin sensitivity. At the same time butyrate is a SCFA that is metabolized in part through the same pathways as long-chain fatty acids. We therefore addressed the effect of butyrate on the mitochondrial oxidation of long- and short-chain fatty acids in C2C12 cells.

Targeted proteomic analysis for proteins in the TCA cycle (Fig. 2A), oxidative phosphorylation (OXPHOS) (Fig. 2B) and β-oxidation (Fig. 2C) revealed a general increase caused by butyrate mainly in the BSA group (Fig. 2A–C). PGC1α, the 'master regulator' of mitochondrial biogenesis [39] was upregulated by either butyrate or palmitate (Fig. 2D). Interestingly, the pyruvate dehydrogenase kinase 4 (PDK4) protein level was higher in palmitate-treated cells (vs BSA), which was further augmented by butyrate treatment in both groups (Fig. 2A, E). A similar pattern was followed by PDK isoforms 1 and 3 (Fig. 2A). PDK inhibits pyruvate dehydrogenase (PDH) and leads to less pyruvate entering the TCA cycle [40]. It is known that an increased lipid supply activates PDK, thus leading to a substrate switch from sugars to fatty acids [40].

Butyrate specifically regulated enzymes involved in butyrate oxidation, such as medium chain ketoacyl-CoA thiolase (MCKAT/ACAA2), and medium- and short-chain acyl-CoA dehydrogenase (MCAD/ACADM and SCAD/ACADS), as well as proteins required for both short- and long-chain fatty-acid oxidation, such as electron-transfer-flavoprotein dehydrogenase (ETFDH) (Fig. 2C). As expected, palmitate induced a general upregulation of the β-oxidation enzymes in the targeted-proteomics panel when compared to the BSA Ctrl (Fig. 2C). CPT1B (muscle isoform), the flux-controlling enzyme for oxidation of specifically long-chain fatty acids [4,29] was too low to be detected in the assay. Palmitate, however, increased the *Cpt1b* mRNA levels by 3-fold compared to the BSA treated group ($p < 0.01$), while butyrate had no significant effect on the *Cpt1b* transcript level (Fig. 2F). The levels of phosphorylated (active) acetyl-CoA carboxylase (ACC), which synthesizes the CPT1B inhibitor malonyl-CoA, were mildly decreased only by palmitate (Fig. S2A). The protein level of CD36, a translocase involved in fatty-acid uptake, was unchanged (Fig. 2G). Total triglyceride (TG)

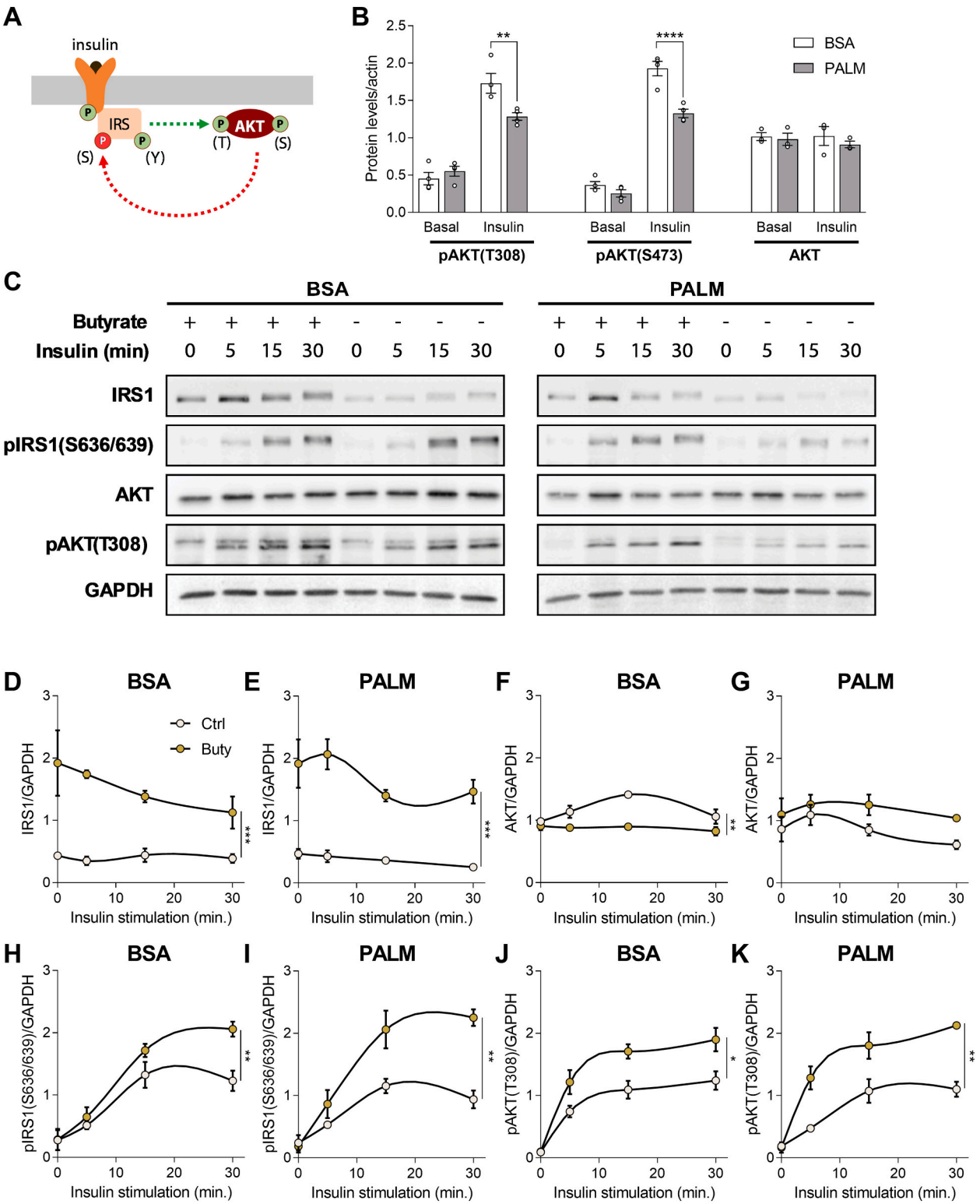

Fig. 1. Butyrate improves insulin sensitivity in a cell model of palmitate-induced insulin resistance. (A) Simplified scheme of IRS1 activation (phosphotyrosine, Y) and inactivation (phosphoserine, S) followed by AKT phosphorylation upon insulin stimulation. (B) pAKT (T308), pAKT (S473) and AKT protein levels (Western Blot) in myotubes treated with either bovine serum albumin (BSA) or BSA-conjugated palmitate (PALM) for 24 h. Cells were incubated with 100 nM insulin for 15 min. (C) Representative time courses of insulin receptor substrate 1 (IRS1), pIRS1(S636/639), protein kinase B (AKT), pAKT(T308) and GAPDH protein levels within 30 min of insulin stimulation. Cells were treated with BSA or PALM in the presence of butyrate (Buty) or control (Ctrl) for 24 h previous to the insulin stimulation. (D–K) Relative quantification of time courses as protein level relative to GAPDH (Western Blot). The data shown are 3–4 independent biological replicates. All data are presented as mean ± SEM. *p < 0.05, **p < 0.01, ***p < 0.001 Ctrl vs Buty.

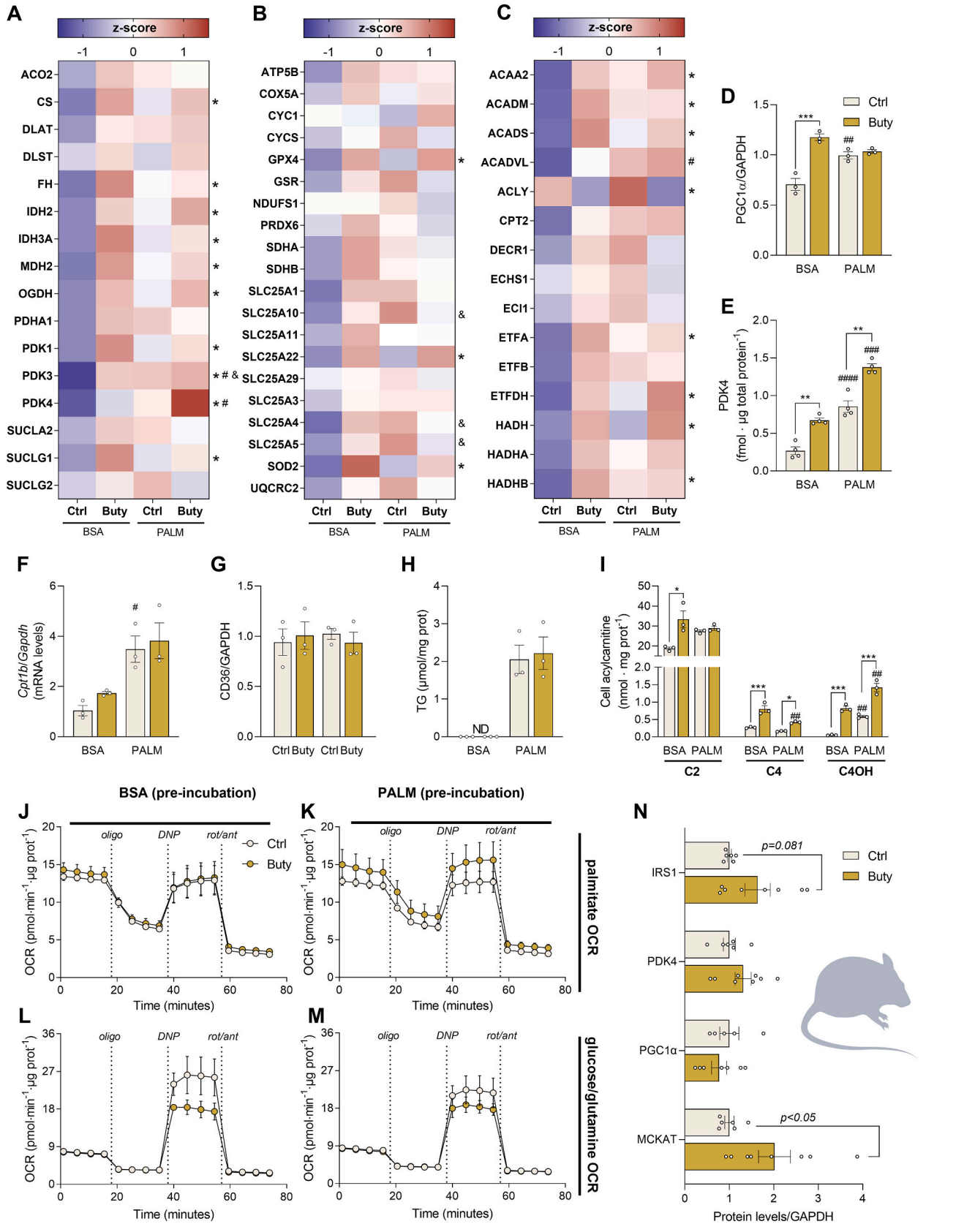

(caption on next page)

Fig. 2. Mitochondrial oxidative capacity is mildly affected by butyrate. Myotubes were treated with either 0.5 % BSA or 500 μM PALM in the presence of Buty or Ctrl for 24 h previous to the analyses described below. Heat map of (A) TCA cycle, (B) ETC and reactive oxygen species detoxification and (C) β-oxidation protein concentrations. Heat maps are based on proteins quantification by targeted proteomics. *Z*-scores were used to normalize the data and protein abbreviations are depicted according to UniProt (Red: high Z-score, upregulated proteins; Blue: low Z-score, downregulated proteins). (D) Peroxisome proliferator-activated receptor gamma coactivator 1-alpha (PGC1α) protein levels relative to GAPDH (Western Blot). (E) Pyruvate dehydrogenase kinase (PDK4) protein from quantitative proteomics. (F) mRNA levels of *Cpt1b* (Carnitine palmitoyltransferase 1B) relative to *Gapdh* levels, (G) fatty-acid translocase (CD36) protein levels relative to GAPDH (Western Blot) and (H) cell triglyceride (TG) incorporation, ND: not detected. (I) Cell acetylcarnitine (C2) butyrylcarnitine (C4) and 3-hydroxy-butyrylcarnitine (C4OH) quantification. Oxygen consumption rates (OCR) in intact cells with either (J, K) palmitate or (L, M) glucose and glutamine as substrates. Cells depicted in (J, L) were pre-incubated with BSA +/− butyrate and cells depicted in (K, M) were pre-incubated with palmitate +/− butyrate. (N) IRS1, PDK4, PGC1α and MCKAT proteins levels relative to GAPDH in the quadriceps of mice fed a high-fat diet supplemented with butyrate (Western Blot). Data are shown as 3–4 independent biological replicates for cell experiments and n = 6–8 for mouse samples. All data are presented as mean ± SEM. *p < 0.05, **p < 0.01, ***p < 0.001 Ctrl vs Buty; $^{\#}$p < 0.05, $^{\#\#}$p < 0.01, $^{\#\#\#}$p < 0.001 BSA vs PALM; $^{\&}$p < 0.05 for interaction between the effects of butyrate and palmitate. (For interpretation of the references to colour in this figure legend, the reader is referred to the web version of this article.)

levels, a measure of lipid accumulation, were strongly enhanced by palmitate, but not affected by butyrate (Fig. 2H).

Palmitate upregulated medium- and long-chain acylcarnitines (C6-C18) (Fig. S2B) in accordance with ongoing palmitate oxidation. Intracellular acetylcarnitine (C2) levels were increased by butyrate only in the BSA group, given that palmitate itself also increased C2 levels (vs BSA) (Fig. 2I). However, butyrate increased acetylcarnitine in both groups when measured in the extracellular medium (Fig. S2C). Butyrate specifically upregulated butyrylcarnitine (C4) and hydroxybutyrylcarnitine (C4OH) >2-fold, irrespective of the presence of palmitate (Fig. 2I). These short-chain acylcarnitines (C2, C4, C4OH) are synthesized by carnitine acetyltransferase (CRAT). *Crat* mRNA levels were upregulated by palmitate, but not by butyrate (Fig. S2D).

To further corroborate the above findings, the actual oxidation fluxes were measured. Pre-treatment with butyrate did not significantly affect palmitate-based oxygen consumption rates (OCR) in intact C2C12 cells (Fig. 2J–K) nor mitochondrial palmitoyl-CoA or palmitoylcarnitine oxidation in permeabilized cells (the latter was tested only in the BSA group; Fig. S2E–F). In contrast, glucose-based respiration showed a tendency (p = 0.08) of lower maximal OCR in intact cells pre-treated with butyrate (uncoupled state, with dinitrophenol, DNP; Fig. 2L–M and S2H), which was confirmed by mitochondrial pyruvate and malate-based respiration in permeabilized cells (Fig. S2G). This agrees with the upregulation of the PDKs by butyrate. Proton leak was approx. 2-fold higher in cells pre-treated with palmitate (Fig. S2H) a known fatty acid uncoupling effect [41], with no further effect by butyrate.

To address if the results could be translated to the skeletal muscle in vivo, mice were fed a high-fat diet supplemented with butyrate. A tendency of higher total IRS1 levels was observed in mice treated with butyrate versus non-treated animals (p = 0.081) (Fig. 2N), together with a decreased fasting glucose concentrations (Fig. S2I). These would indicate improved insulin sensitivity, as previously reported for in vivo butyrate treatment [19]. These were also accompanied by an upward trend in PDK4. In parallel, no changes in total PGC1α were detected, which aligns with the results in the palmitate group in the C2C12 cells. Finally, a circa 2-fold increase in MCKAT was induced by butyrate (Fig. 2N).

Together, the results show that butyrate and palmitate are metabolized by muscle cells, where butyrate induces expression of butyrate-metabolizing enzymes, but not of enzymes dedicated to long-chain fatty-acid metabolism. Furthermore, upregulation of PDK by butyrate suggests that butyrate serves as an alternative substrate at the expense of carbohydrates.

3.3. Butyrate-simulated insulin signalling is enhanced by inhibition of butyrate metabolism

Butyrate is a known inhibitor of HDACs, which increases histone acetylation and thereby induces gene transcription [21,42]. Since butyrate was also actively metabolized by the C2C12 muscle cells, we wondered if butyrate catabolism contributed to its effect on insulin signalling. To address this, we generated a stable knockdown of the *Acaa2* gene encoding MCKAT in C2C12 myotubes. MCKAT catalyses the final step of the oxidation of short-chain fatty acids, in which a 3-keto-butyryl-CoA is converted into 2 acetyl-CoA molecules (Fig. 3A). The enzyme is essential for the oxidation of butyrate as well as for the last cycles of the complete oxidation of palmitate, for which it may contribute to the control of flux [4,31].

The knockdown efficiency was around 95 % at both mRNA (Fig. 3B) and protein level (Fig. 3C) and did not change after butyrate treatment (Fig. S3A). Neither differentiation into myotubes, assessed by myogenic markers *Myod1*, *Myog* and *Ckm* (Fig. S3B), nor cell viability (Fig. S3C) was affected by *Acaa2* knockdown and empty vector, when compared to the wild type (WT). In the butyrate groups, the knockdown of *Acaa2* did not affect the concentration of butyrylcarnitine (Fig. 3D). However, in the BSA group treated with butyrate, *Acaa2* knockdown did increase C4OH-carnitine, a metabolite more closely upstream of MCKAT, by twofold versus the empty vector (Fig. 3E). This is consistent with a decreased MCKAT activity. Along the same lines, in the palmitate group the *Acaa2* knockdown caused accumulation of another upstream metabolite, C6-carnitine (Fig. 3F; complete acylcarnitine profile: Table S1).

In the *Acaa2* knockdown cells, butyrate increased the total IRS1 (Fig. 3G) to a similar extent as in the empty vector (Fig. 1D–E), demonstrating that the stimulation of insulin signalling by butyrate does not depend on butyrate metabolism. Conspicuously, total IRS1 levels and butyrate stimulation thereof were very low in the empty vector (Fig. 3G). Thus, compared to the empty vector, stimulation by butyrate was even enhanced in the *Acaa2* knockdown. After 15 min of insulin stimulation, the levels of pAKT(T308) were somewhat higher in the *Acaa2* knockdown than in the empty vector ($p_{genotype} < 0.01$) (Fig. 3H, S3J), whereas pIRS1(S636/639) followed the same pattern as IRS1 (Fig. S3D, F-G). The levels of and pIRS1(Y612), a residue necessary for IRS1 activation and therefore a further marker of insulin sensitivity, was also increased by butyrate and higher in the Acaa2 knockdown than in the empty vector (Sig. S3E–F, H). Total AKT levels were constant under all conditions, (Fig. 3I, S3I), as previously observed (Fig. 1F–G). Together, the results suggest that inhibiting butyrate catabolism indirectly stimulates insulin signalling.

3.4. Butyrate stimulates glycolysis in palmitate-treated cells

Whereas the increase of insulin sensitivity by butyrate would increase the consumption of glucose, the upregulation of the PDKs would redirect glucose towards lactate. We therefore quantified extracellular acidification rates (ECAR) with glucose as the substrate (Fig. 4A) as a functional readout for glucose uptake and subsequent metabolism (dependent on IRS1, pAKT and GLUT4). Butyrate indeed increased the basal and maximal glycolytic capacity in palmitate-treated myotubes (by ~50 %) when pre-stimulated with insulin (Fig. 4B–E, G). Targeted proteomics (Fig. 4F) showed that total levels of hexokinase (HK) and phosphofructokinase (PFK), known nodes of glycolytic flux control [43–45], were unchanged among groups (Fig. S4A–B). Instead, the enzyme 6-phosphofructo-2-kinase/fructose-2,6-bisphosphatase 2

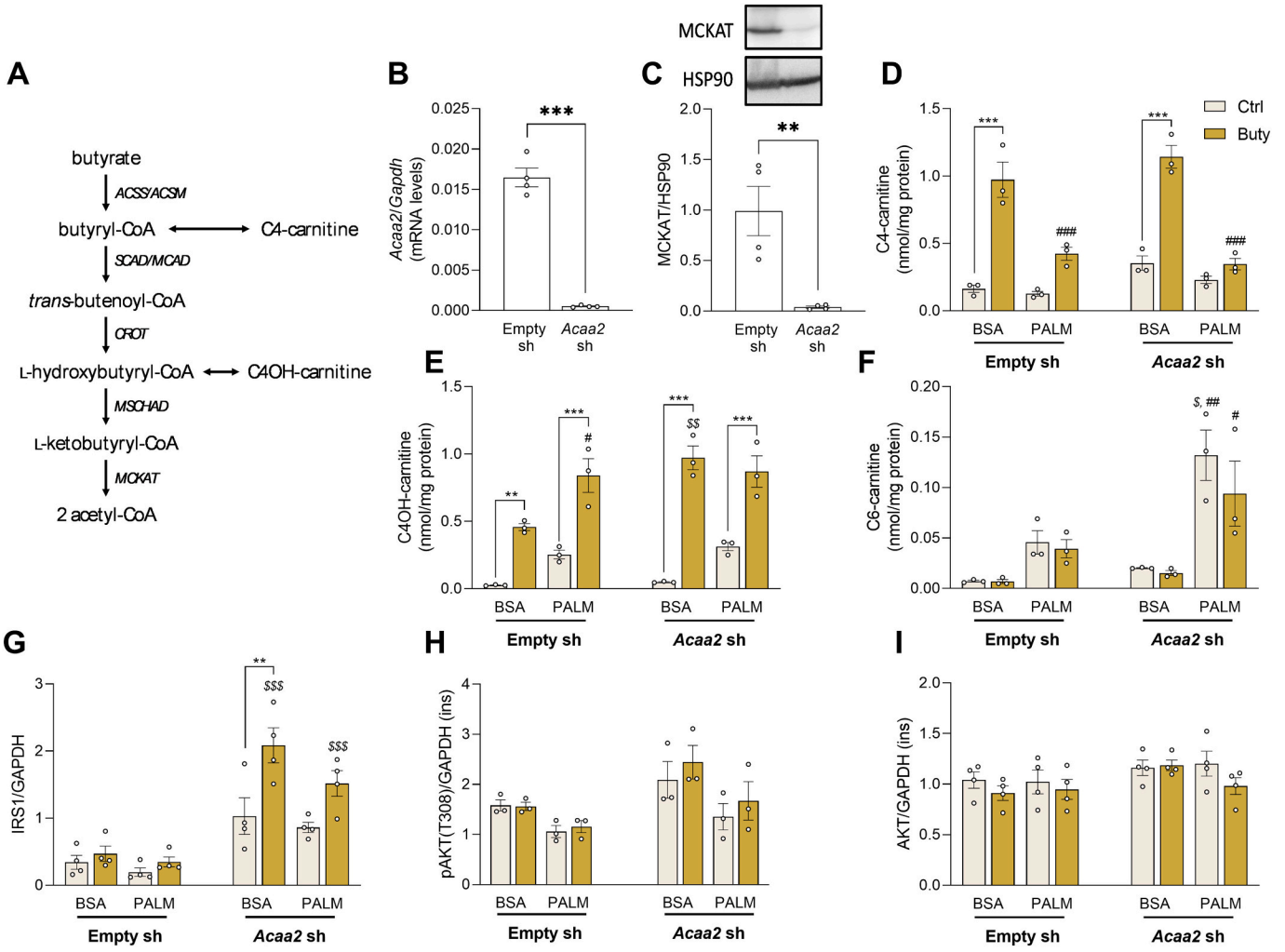

Fig. 3. Butyrate effects on insulin signalling are connected to its metabolization. (A) Schematic view of butyrate catabolism pathway. ACSM: medium-chain acyl-CoA synthetase, ACSS: short-chain acyl-CoA synthetase, MCAD: medium-chain acyl-CoA dehydrogenase, SCAD: short-chain acyl-CoA dehydrogenase, CROT: enoyl-CoA hydratase/crotonase, MSCHAD: medium and short-chain 3-hydroxyacyl-CoA dehydrogenase, MCKAT: medium-chain 3-ketoacyl-CoA thiolase/acetyl-CoA acetyltransferase (ACAA2). (B) mRNA levels relative to *Gapdh* and (C) MCKAT protein levels relative to heat shock protein 90 (HSP90) levels (Western Blot) and representative image in differentiated myotubes. *Acaa2* knockdown (*Acaa2* sh) C2C12 myotubes and the empty vector (Empty sh) were treated with 0.5 % BSA or 500 μM PALM in the presence of Buty or Ctrl for 24 h previously to the analyses described below. (D) Cell butyrylcarnitine (C4), (E) 3-hydroxy-butyrylcarnitine (C4OH) and (F) hexanoylcarnitine (C6) quantification. (G) IRS1 protein levels relative to GAPDH (Western Blot). (H) pAKT (T308) protein levels (I) and total AKT levels relative to GAPDH after 15 min of insulin stimulation (Western Blot). The data shown are 3–4 independent biological replicates. All data are presented as mean ± SEM. $^{*}p < 0.05$, $^{**}p < 0.01$, $^{***}p < 0.001$ Ctrl vs Buty; $^{\#}p < 0.05$, $^{\#\#}p < 0.01$, $^{\#\#\#}p < 0.001$ BSA vs PALM; $^{\&}p < 0.05$ for interaction between the effects of butyrate and palmitate and $^{\$}p < 0.05$, $^{\$\$}p < 0.01$, $^{\$\$\$}p < 0.001$ *Acaa2* knockdown vs empty vector.

(PFKFB2) was upregulated by butyrate exclusively in the insulin-stimulated palmitate group, thus showing the same pattern as the ECAR (Fig. 4F, H). The PFKFB2 isoform is the most abundant in C2C12 cells [46]. It is a bifunctional enzyme that produces and degrades fructose-2,6-bisphosphate, an allosteric activator of phosphofructokinase. The kinase activity, responsible for fructose-2,6-bisphosphate production, is stimulated by insulin. To test whether there was a causal relationship between the PFKFB2 level and the ECAR, we generated a *Pfkfb2* knockdown in C2C12 cells. We obtained only 37 % reduction of the protein level (Fig. S4C) with no change in viability (Fig. S3C). Interestingly, in the presence of butyrate the PFKFB2 level in the knockdown strain was comparable to that of the empty vector in the absence of butyrate (Fig. S4C). Despite this normalized PFKFB2 level the butyrate-stimulated *Pfkfb2* knockdown line showed a higher maximal ECAR than the empty vector in the insulin-treated group (Fig. S4D–E), suggesting that PFKFB2 is not causally involved in the upregulation of ECAR by butyrate. In view of these mild effects, a possible role of PFKFB2 cannot, however, be completely excluded.

Depending on the conditions, the transporters of glucose and lactate also exert considerable control over glycolytic flux [43]. Butyrate increased the mRNA levels of the insulin-responsive transporter *Slc2a4* (GLUT4) and of the monocarboxylate transporter 1 *Slc16a1* (MCT-1) (Fig. 4I). MCT-1 is responsible for the uptake of butyrate as well as the export of lactate [47], and is the most abundant MCT in C2C12 cells [48]. *Slc2a1* mRNA, encoding the insulin-independent glucose transporter GLUT1, was not significantly affected by butyrate (Fig. 4I).

3.5. *Inhibition of butyrate oxidation magnifies HDAC-dependent butyrate induction of glycolysis*

We next investigated whether the stimulation of glycolysis and the upregulation of the transporters by butyrate were dependent on butyrate catabolism. Butyrate-treated *Acaa2* knockdown cells exhibited a higher insulin-stimulated glycolytic capacity than the empty vector (Fig. 4J). No difference between the *Acaa2* knockdown and the empty vector were observed in the absence of insulin (Fig. S4F). Butyrate also increased

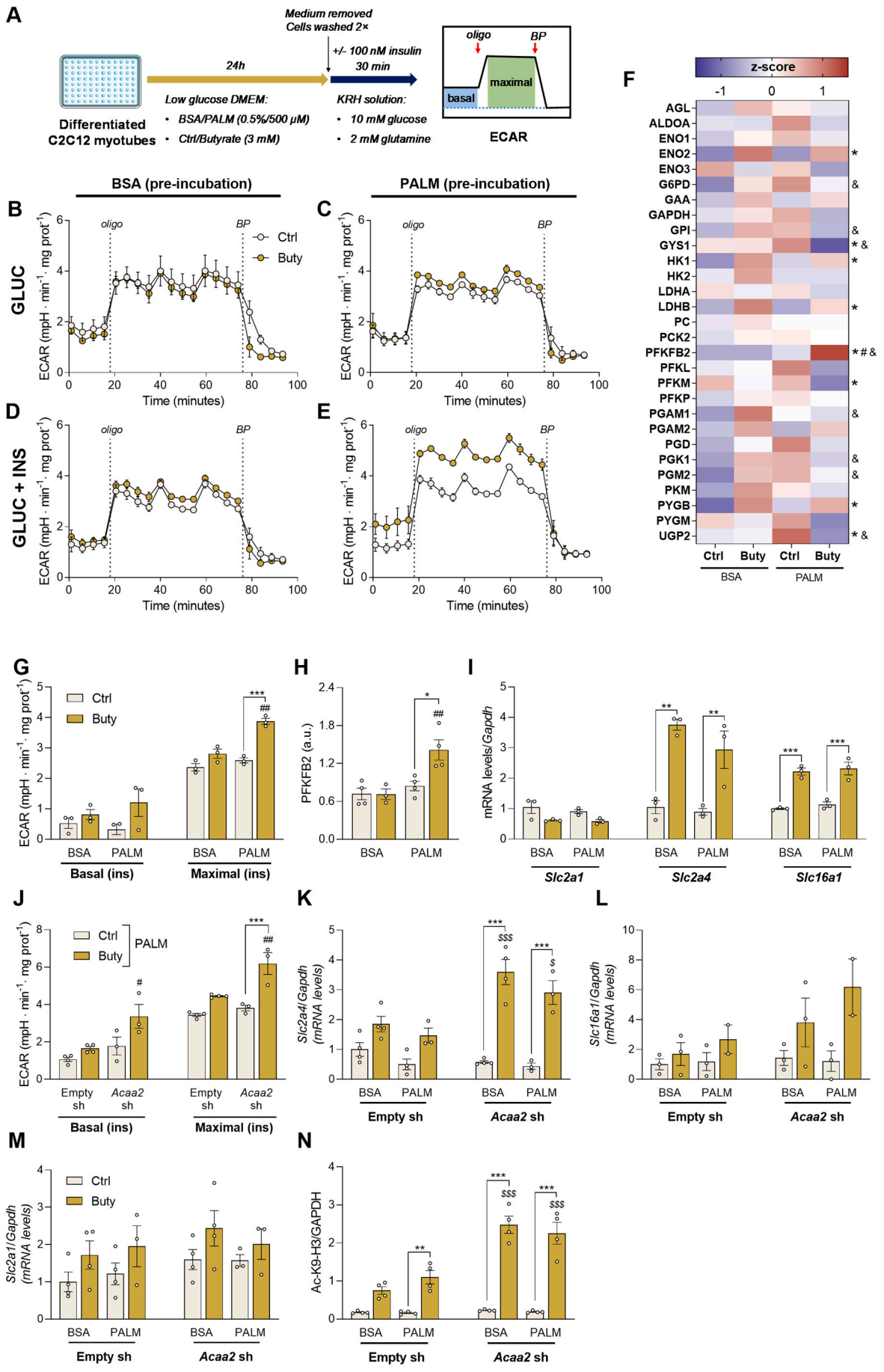

(caption on next page)

Fig. 4. Butyrate metabolism affects glycolysis in palmitate-treated cells. Myotubes were treated with either 0.5 % BSA or 500 μM PALM in the presence of Buty or Ctrl for 24 h previously to the analyses described below. (A) schematic visualization of the experimental setup to measure extracellular acidification rates (ECAR). Oligo: oligomycin injection, BP: bromopyruvate injection. (B-E) ECAR over time with glucose as substrate, without (B, C) or with (D, E) insulin stimulation starting 30 min prior to measurements. (F) Heat map of glycolytic protein levels quantified with targeted proteomics. *Z*-scores were used to normalize the data and protein abbreviations are depicted according to UniProt (Red: high Z-score, upregulated proteins; Blue: low Z-score, downregulated proteins). (G) Quantification of basal and maximal glycolytic capacity from ECAR data. (H) PFKFB2 protein levels normalized to GAPDH levels in C2C12 cells, obtained from proteomics. (I) mRNA levels of *Slc2a1* (GLUT1), *Slc2a4* (GLUT4) and *Slc16a1* (MCT-1) relative to *Gapdh*. (J) Quantification of basal and maximal glycolytic capacity from ECAR data from *Acaa2* knockdown (*Acaa2* sh) myotubes and the empty vector (Empty sh) with the use of glucose as substrate in the presence of insulin. mRNA levels of (K) *Slc2a4* (GLUT4), (L) *Slc16a1* (MCT-1) and (M) *Slc2a1* (GLUT1) relative to *Gapdh* in *Acaa2* knockdown and control myotubes. (N) Acetylation of histone 3 protein at Lys 9 (Ac-K9-H3) relative to GAPDH (Western Blot) in *Acaa2* knockdown and control myotubes. Data are shown as 3–4 independent biological replicates. All data are presented as mean ± SEM. $^{*}p < 0.05$, $^{**}p < 0.01$, $^{***}p < 0.001$ Ctrl vs Buty; $^{\#}p < 0.05$, $^{\#\#}p < 0.01$, $^{\#\#\#}p < 0.001$ BSA vs PALM; $^{\&}p < 0.05$ for interaction between the effects of butyrate and palmitate and $^{\$}p < 0.05$, $^{\$\$}p < 0.01$, $^{\$\$\$}p < 0.001$ *Acaa2* knockdown vs empty vector. (For interpretation of the references to colour in this figure legend, the reader is referred to the web version of this article.)

Slc2a4 and *Slc16a1* transcription to a higher extent in the *Acaa2* knockdown than in the empty vector (Fig. 4K–L), but not that of *Slc2a1* (GLUT1) (Fig. 4M). The stronger effects of butyrate on glycolytic and transport capacity in the *Acaa2* knockdown was consistent with a stronger HDAC inhibition, as evidenced by the higher levels of acetylated histone 3 (a target of HDAC) in butyrate-treated *Acaa2* knockdown versus the empty vector cells (Fig. 4N). In line with the results shown in vitro, Ac-K9-H3 in the mouse quadriceps showed a tendency of higher levels in the butyrate-treated group versus control (Fig. S4G). In general, all in vivo results in mouse had the same tendency as the results in vitro, but to a lesser extent. Interestingly, the levels of IRS1 correlated with the intensity of histone 3 acetylation (Fig. S4H, $R^2 = 0.64$, $p < 0.001$), which is consistent with the literature evidence that IRS1 is regulated by butyrate via gene expression. In conclusion, the results indicate that butyrate enhanced maximal insulin-stimulated glycolytic capacity via upregulation of GLUT4 and MCT-1 likely in an HDAC-dependent manner.

4. Discussion

Butyrate administration has been linked to improved peripheral insulin sensitivity in mice [11,12,49] and in humans [50]. Here, we studied the underlying mechanism in palmitate-treated myotubes as an in vitro model for lipid-induced insulin resistance. In the myotubes, butyrate indeed increased the levels of insulin signalling proteins IRS1 and pAKT and enhanced glycolytic capacity. In vivo observations were largely recapitulated in vitro, in agreement with a direct effect of butyrate on the muscle. Contrary to our expectations, butyrate did not affect mitochondrial long-chain fatty-acid oxidation. It did, however, increase the levels of proteins and metabolites involved in butyrate oxidation itself. By inhibiting butyrate oxidation, the butyrate-induced cellular remodelling was amplified. This shows that butyrate oxidation is not required for its insulin-sensitizing effect. Rather the opposite: inhibition of butyrate metabolism probably increases its intracellular concentration, leading to an enhanced HDAC inhibition. To our knowledge this is the first integrated study of butyrate metabolism and butyrate-dependent transcription regulation in muscle cells, revealing unexpected interactions between these two mechanisms in the context of insulin signalling and glucose metabolism.

Oral butyrate administration increases peripheral insulin sensitivity in mice [11,12]. The skeletal muscle is a key contributor to glucose clearance in the body [51]. Gao et al. showed elevated phosphorylation of IRS1 and AKT in the skeletal muscle of mice treated with butyrate [12]. Higher IRS1 levels were also observed in L6 cells treated with butyrate [24]. We confirmed increased IRS1 levels and consequent increased pAKT levels in vitro in C2C12 myotubes treated with butyrate (Fig. 1C–E, J–K), in line with a direct effect on the muscle. Butyrate enhanced IRS1 levels via HDAC inhibition [24]. Other HDAC inhibitors or *Hdac5* knockout showed similar effects on insulin signalling and insulin-stimulated glucose uptake in skeletal muscle or cultured myotubes [24,52–54]. In vitro studies typically apply supra-physiological concentrations of butyrate, and ours is no exception. Although peripheral concentrations of butyrate are typically in the μM range [12,14,55,56], orally administered butyrate may reach plasma concentrations of >1 mM [57], in the range of the K_i of HDAC for butyrate [24,58]. HDAC inhibition (genetic or pharmacologic) enhances *Slc2a4* expression [23,54,59] and glycolysis [52] in muscle cells. This aligns with the effects elicited by butyrate in the present study (Fig. 4E, G, I). Thus, the observed effects on insulin signalling may in principle be explained by HDAC inhibition alone.

When we focus downstream of insulin signalling at glucose metabolism, the most intriguing observation was that butyrate enhanced the insulin-stimulated glycolytic flux only in the palmitate-group (Fig. 4E, G), despite the upregulation of *Slc2a4* and *Slc16a1* and PDK4 in both palmitate and BSA groups (Figs. 2E and 4I). The regulatory enzyme PFKFB2 followed the same pattern as the glycolytic capacity, but knocking down this enzyme suggested no direct causal relation (Fig. S4C, E). An upregulation of the glucose-to-lactate pathway (ECAR) by palmitate has been reported before and was then linked to palmitate-induced H_2O_2 production and a more oxidized $NAD(P)^+$/NAD(*P*)H pool [60]. It is conceivable that the combination of butyrate and palmitate in our study led to a further oxidative imbalance, thus boosting the ECAR. Kakimoto et al. showed that specific scavenging of mitochondrial ROS did, however, not reduce the ECAR [60], making it difficult to investigate this mechanism further in the context of butyrate.

There is evidence that increased mitochondrial oxidative capacity contributes to insulin sensitivity through a faster clearance of lipid species [5,6,61,62]. Multiple in vivo studies have shown that butyrate supplementation reduces the respiratory exchange ratio (i.e. CO_2 production rate divided by O_2 consumption rate) [11,12,19,63], indicative of an increased systemic fatty-acid oxidation relative to glucose oxidation. In line with the latter, butyrate-treated C2C12 cells showed a tendency of lower maximal oxidative capacity with glucose or pyruvate as substrates (Fig. 2L, M and S2G). This could be attributed to the observed increase of PDK4 in response to butyrate (Fig. 2E). PDK4 regulates the entry of pyruvate into mitochondrial metabolism and thereby the rate of glucose oxidation, leading to a switch towards other substrates such as fatty acids for oxidation. The capacity to oxidize long-chain fatty-acids was unchanged (Fig. 2J–K and S2E–F). This was surprising, given that Gao et al. reported increased $^{14}CO_2$ release from labelled palmitate oxidation both ex vivo and in vitro [12], which aligned with butyrate-induced upregulation of PGC1α and CPT1B [12,25–27]. In the C2C12 cells the upregulation of PGC1α and a tendency of higher *Cpt1b* was observed only in cells treated with butyrate in the absence of palmitate (Fig. 2D, F). Interestingly, in the C2C12 cells butyrate did increase the levels of short/medium-chain fatty-acid oxidation enzymes, among which MCKAT (Fig. 2C), and of C2-, C4- and C4OH-carnitine (Fig. 2I), indicating an upregulation of butyrate oxidation itself. The increased MCKAT levels in the quadriceps of butyrate-treated mice (Fig. 2N) suggest that the same phenomenon takes place in vivo.

After we observed that butyrate was actively metabolized, we addressed how this affected insulin sensitivity by knocking down *Acaa2* (Fig. 3B, C). The increased concentrations of upstream metabolites

confirmed the desired effect on inhibiting butyrate metabolism (Fig. 3D–E, Table S1). Conspicuously, butyrate-induced IRS1 and *Slc2a4* upregulation was exacerbated in the *Acaa2* knockdown (Figs. 3G, 4K). Moreover, when measuring ECAR as a functional assay of glucose metabolism, we showed that the *Acaa2* knockdown cells exhibited a higher basal glycolytic rate, which was further increased by the butyrate treatment (Fig. 4J). This was accompanied by a substantially increased of H3 K9-acetylation when butyrate oxidation was inhibited (Fig. 4K, N). The elevated histone acetylation level and its downstream effects, suggest a more potent HDAC inhibition in the *Acaa2* knockdown cells (Fig. 5). We therefore hypothesize that butyrate oxidation decreases intracellular butyrate availability and consequently decreases HDAC inhibition. Inhibiting this oxidation pathway in the presence of administered butyrate would, in turn, lead to increased expression of target genes that improve insulin sensitivity. It is important to mention that both processes, butyrate oxidation and inhibition of HDAC by butyrate, will occur in the cell simultaneously. It is the balance between these processes that determines the net effect.

Skeletal muscle mitochondria also contain acetyl-CoA acetyltransferase (ACAT1) [64], which catalyses the same reversible reaction as MCKAT (ACAA2) and is involved in branched-chain amino acid catabolism and ketone body utilization [65]. Therefore, we cannot exclude that butyrate oxidation could still partially follow this route in the *Acaa2* knockdown. Furthermore, it has been reported that MCKAT and other enzymes involved in the oxidation of short-chain fatty acids localize partly to the nucleus. There, they modulate the availability of butyryl-CoA for histone butyrylation [66], a less explored histone modification that may induce gene transcription (Trefely et al., 2020). How intracellular butyrate availability and histone butyrylation affect insulin sensitivity, remains a topic for further study.

The present study comprehensively addresses the mechanism by which butyrate improves insulin sensitivity in the skeletal muscle. Limitations of the study are (1) that we addressed glucose transport only at the mRNA level and indirectly via ECAR; (2) that we focused on butyrate supplementation only as a prevention strategy and not on butyrate treatment to restore insulin resistance. Butyrate as a treatment strategy against IR has been previously demonstrated in mice [11], although a direct effect on muscle physiology has not been addressed and represents a logical follow-up to the current study. Finally, (3) butyrate enhances the glycolytic capacity of C2C12 myotubes only in the presence of palmitate, which was hypothesized to be mediated by PFKFB2. However, the results were not conclusive to confirm or reject this hypothesis.

5. Conclusions

C2C12 myotubes represent a valuable model to investigate the multilayered effects of butyrate on lipid-induced insulin sensitivity in the skeletal muscle. In contrast to earlier findings, butyrate did not affect long-chain fatty-acid oxidation, suggesting that the effect of the SCFA on gene expression alone is sufficient to improve insulin sensitivity in vitro. Inhibition of butyrate oxidation exacerbated its effect on insulin sensitivity, likely increasing both butyrate availability and HDAC inhibition. In vivo butyrate-induced increased insulin sensitivity does not only depend on the skeletal muscle, but also on other tissues, notably liver and adipose. The interplay between butyrate metabolism and histone modification may therefore also be relevant for other tissues. Understanding how butyrate modulates multiple intracellular pathways in a concerted manner could aid the development of novel treatment strategies towards preventing and treating insulin resistance.

Funding

This study was supported by a UMCG-GSMS PhD fellowship, the De Cock-Hadders Foundation and the UMCG Hereditary Metabolic Diseases Fund.

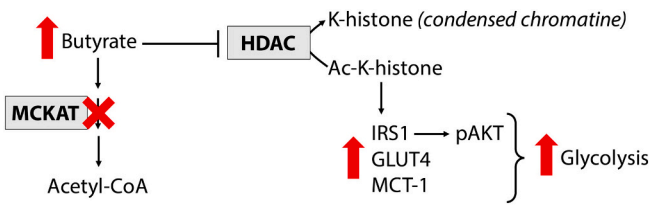

Fig. 5. Schematic overview of suggested mechanism of butyrate (oxidation) on muscle insulin sensitivity. Butyrate is oxidized via the short-/medium-chain branch of the mitochondrial fatty-acid oxidation to produce acetyl-CoA. Butyrate also inhibits HDAC. This leads to a higher status of histone acetylation, which induces the transcription of selected targets, such as *Irs1, Slc2a4* (GLUT4) and *Slc16a1* (MCT-1). Increased protein levels of IRS1 leads to higher AKT phosphorylation, which, together with enhanced GLUT4 and MCT-1 levels, results in a higher insulin-stimulated glycolytic capacity. The degree of HDAC inhibition by butyrate depends on its intracellular concentration, which in turn depends on the balance between uptake and oxidation fluxes. Inhibition of butyrate oxidation by MCKAT downregulation (red cross) raises the concentration of butyrate and enhances its ability to inhibit HDAC. This amplifies its target effects on insulin sensitivity. (For interpretation of the references to colour in this figure legend, the reader is referred to the web version of this article.)

CRediT authorship contribution statement

Melany Rios-Morales: Conceptualization, Data curation, Formal analysis, Funding acquisition, Investigation, Methodology, Visualization, Writing – original draft. **Marcel A. Vieira-Lara:** Conceptualization, Data curation, Formal analysis, Funding acquisition, Investigation, Methodology, Visualization, Writing – original draft. **Esther Homan:** Formal analysis, Investigation. **Miriam Langelaar-Makkinje:** Formal analysis, Investigation. **Albert Gerding:** Formal analysis, Investigation. **Zhuang Li:** Investigation, Methodology. **Nicolette Huijkman:** Methodology. **Patrick C.N. Rensen:** Investigation, Supervision, Funding acquisition. **Justina C. Wolters:** Formal analysis, Investigation, Methodology. **Dirk-Jan Reijngoud:** Investigation, Supervision, Funding acquisition. **Barbara M. Bakker:** Investigation, Supervision, Funding acquisition, Writing – review & editing.

Declaration of competing interest

None.

Acknowledgements

We would like to thank Bart van de Sluis for the input provided for the generation of the knockdown cell lines and Debby Koonen for bridging the collaboration with Leiden University Medical Center.

Appendix A. Supplementary data

Supplementary data to this article can be found online at https://doi.org/10.1016/j.bbadis.2022.166476.

References

[1] M.C. Petersen, G.I. Shulman, Mechanisms of insulin action and insulin resistance, Physiol. Rev. 98 (4) (2018) 2133–2223.
[2] P.J. Meikle, S.A. Summers, Sphingolipids and phospholipids in insulin resistance and related metabolic disorders, Nat Rev Endocrinol 13 (2) (2017) 79–91.
[3] P.A. Watkins, D. Maiguel, Z. Jia, J. Pevsner, Evidence for 26 distinct acyl-coenzyme a synthetase genes in the human genome, J. Lipid Res. 48 (12) (2007) 2736–2750.
[4] S. Eaton, Control of mitochondrial β-oxidation flux, Prog. Lipid Res. 41 (3) (2002) 197–239.
[5] C.R. Bruce, A.J. Hoy, N. Turner, M.J. Watt, T.L. Allen, K. Carpenter, et al., Overexpression of carnitine palmitoyltransferase-1 in skeletal muscle is sufficient to enhance fatty acid oxidation and improve high-fat diet-induced insulin resistance, Diabetes 58 (3) (2009) 550–558.

[6] J.H. Koh, M.L. Johnson, S. Dasari, N.K. LeBrasseur, I. Vuckovic, G.C. Henderson, et al., TFAM enhances fat oxidation and attenuates high fat diet induced insulin resistance in skeletal muscle, Diabetes 68 (8) (2019) 1552–1564.
[7] E.E. Canfora, J.W. Jocken, E.E. Blaak, Short-chain fatty acids in control of body weight and insulin sensitivity, Nat Rev Endocrinol 11 (10) (2015) 577–591.
[8] A. Koh, F. De Vadder, P. Kovatcheva-Datchary, F. Bäckhed, From dietary fiber to host physiology: short-chain fatty acids as key bacterial metabolites, Cell 165 (6) (2016) 1332–1345.
[9] G. den Besten, R. Havinga, A. Bleeker, S. Rao, A. Gerding, K. van Eunen, et al., The short-chain fatty acid uptake fluxes by mice on a guar gum supplemented diet associate with amelioration of major biomarkers of the metabolic syndrome, PLoS ONE 9 (9) (2014), e107392.
[10] E.E. Blaak, E.E. Canfora, S. Theis, G. Frost, A.K. Groen, G. Mithieux, et al., Short chain fatty acids in human gut and metabolic health, Benef Microbes 11 (5) (2020) 411–455.
[11] G. den Besten, A. Bleeker, A. Gerding, K. van Eunen, R. Havinga, T.H. van Dijk, et al., Short-chain fatty acids protect against high-fat diet-induced obesity via a PPARγ-dependent switch from lipogenesis to fat oxidation, Diabetes 64 (7) (2015) 2398–2408.
[12] Z. Gao, J. Yin, J. Zhang, R.E. Ward, R.J. Martin, M. Lefevre, et al., Butyrate improves insulin sensitivity and increases energy expenditure in mice, Diabetes 58 (7) (2009) 1509–1517.
[13] A. Vrieze, E. Van Nood, F. Holleman, J. Salojärvi, R.S. Kootte, J.F.W. M. Bartelsman, et al., Transfer of intestinal microbiota from lean donors increases insulin sensitivity in individuals with metabolic syndrome, Gastroenterology 143 (4) (2012) 913–916.e917.
[14] E.E. Canfora, C.M. van der Beek, J.W.E. Jocken, G.H. Goossens, J.J. Holst, S.W. M. Olde Damink, et al., Colonic infusions of short-chain fatty acid mixtures promote energy metabolism in overweight/obese men: a randomized crossover trial, Sci. Rep. 7 (1) (2017) 2360.
[15] J.W.E. Jocken, M.A. González Hernández, N.T.H. Hoebers, C.M. van der Beek, Y.P. G. Essers, E.E. Blaak, et al., Short-chain fatty acids differentially affect intracellular lipolysis in a human white adipocyte model, Front. Endocrinol. 8 (372) (2018).
[16] A. Girousse, G. Tavernier, C. Valle, C. Moro, N. Mejhert, A.-L. Dinel, et al., Partial inhibition of adipose tissue lipolysis improves glucose metabolism and insulin sensitivity without alteration of fat mass, PLoS Biol. 11 (2) (2013), e1001485.
[17] A. Veprik, D. Laufer, S. Weiss, N. Rubins, M.D. Walker, GPR41 modulates insulin secretion and gene expression in pancreatic β-cells and modifies metabolic homeostasis in fed and fasting states, FASEB J. 30 (11) (2016) 3860–3869.
[18] J.C. McNelis, Y.S. Lee, R. Mayoral, R. van der Kant, A.M. Johnson, J. Wollam, et al., GPR43 potentiates β-cell function in obesity, Diabetes 64 (9) (2015) 3203–3217.
[19] Z. Li, C.X. Yi, S. Katiraei, S. Kooijman, E. Zhou, C.K. Chung, et al., Butyrate reduces appetite and activates brown adipose tissue via the gut-brain neural circuit, Gut 67 (7) (2018) 1269–1279.
[20] B. Dalile, L. Van Oudenhove, B. Vervliet, K. Verbeke, The role of short-chain fatty acids in microbiota-gut-brain communication, Nat Rev Gastroenterol Hepatol 16 (8) (2019) 461–478.
[21] K. Steliou, M.S. Boosalis, S.P. Perrine, J. Sangerman, D.V. Faller, Butyrate histone deacetylase inhibitors, BioResearch open access 1 (4) (2012) 192–198.
[22] J.R. Davie, Inhibition of histone deacetylase activity by butyrate, J. Nutr. 133 (7) (2003) 2485S–2493S.
[23] S. Raichur, S.H. Teh, K. Ohwaki, V. Gaur, Y.C. Long, M. Hargreaves, et al., Histone deacetylase 5 regulates glucose uptake and insulin action in muscle cells, J. Mol. Endocrinol. 49 (3) (2012) 203–211.
[24] S. Chriett, O. Zerzaihi, H. Vidal, L. Pirola, The histone deacetylase inhibitor sodium butyrate improves insulin signalling in palmitate-induced insulin resistance in L6 rat muscle cells through epigenetically-mediated up-regulation of Irs1, Mol. Cell. Endocrinol. 439 (2017) 224–232.
[25] S. Chriett, A. Dabek, M. Wojtala, H. Vidal, A. Balcerczyk, L. Pirola, Prominent action of butyrate over beta-hydroxybutyrate as histone deacetylase inhibitor, transcriptional modulator and anti-inflammatory molecule, Sci. Rep. 9 (1) (2019) 742.
[26] J. Hong, Y.M. Jia, S. Pan, L.F. Jia, H.F. Li, Z.Q. Han, et al., Butyrate alleviates high fat diet-induced obesity through activation of adiponectin-mediated pathway and stimulation of mitochondrial function in the skeletal muscle of mice, Oncotarget 7 (35) (2016) 56071–56082.
[27] T.M. Henagan, B. Stefanska, Z. Fang, A.M. Navard, J. Ye, N.R. Lenard, et al., Sodium butyrate epigenetically modulates high-fat diet-induced skeletal muscle mitochondrial adaptation, obesity and insulin resistance through nucleosome positioning, Br. J. Pharmacol. 172 (11) (2015) 2782–2798.
[28] S. Lahiri, H. Kim, I. Garcia-Perez, M.M. Reza, K.A. Martin, P. Kundu, et al., The gut microbiota influences skeletal muscle mass and function in mice, Sci. Transl. Med. 11 (502) (2019).
[29] S.M. Astbury, B.M. Corfe, Uptake and metabolism of the short-chain fatty acid butyrate, a critical review of the literature, Curr. Drug Metab. 13 (6) (2012) 815–821.
[30] M. Westerterp, C.C. van der Hoogt, W. de Haan, E.H. Offerman, G.M. Dallinga-Thie, J.W. Jukema, et al., Cholesteryl ester transfer protein decreases high-density lipoprotein and severely aggravates atherosclerosis in APOE*3-Leiden mice, Arterioscler. Thromb. Vasc. Biol. 26 (11) (2006) 2552–2559.
[31] M.A. Vieira-Lara, M.B. Dommerholt, W. Zhang, M. Blankestijn, J.C. Wolters, F. Abegaz, et al., Age-related susceptibility to insulin resistance arises from a combination of CPT1B decline and lipid overload, BMC Biol. 19 (1) (2021) 154.
[32] A.M. Heberle, P. Razquin Navas, M. Langelaar-Makkinje, K. Kasack, A. Sadik, E. Faessler, et al., The PI3K and MAPK/p38 pathways control stress granule assembly in a hierarchical manner, Life Sci. Alliance 2 (2) (2019).
[33] V. Bodart, M. Febbraio, A. Demers, N. McNicoll, P. Pohankova, A. Perreault, et al., CD36 mediates the cardiovascular action of growth hormone-releasing peptides in the heart, Circ. Res. 90 (8) (2002) 844–849.
[34] J.C. Wolters, J. Ciapaite, K. van Eunen, K.E. Niezen-Koning, A. Matton, R.J. Porte, et al., Translational targeted proteomics profiling of mitochondrial energy metabolic pathways in mouse and human samples, J. Proteome Res. 15 (9) (2016) 3204–3213.
[35] T.G. Derks, T.S. Boer, A. van Assen, T. Bos, J. Ruiter, H.R. Waterham, et al., Neonatal screening for medium-chain acyl-CoA dehydrogenase (MCAD) deficiency in the Netherlands: the importance of enzyme analysis to ascertain true MCAD deficiency, J. Inherit. Metab. Dis. 31 (1) (2008) 88–96.
[36] E.G. Bligh, W.J. Dyer, A rapid method of total lipid extraction and purification, Can. J. Biochem. Physiol. 37 (1) (1959) 911–917.
[37] E. Gnaiger, V. Kuznetsov, S. Schneeberger, R. Seiler, G. Brandacher, W. Seteurer, et al., Mitochondria in the cold, in: S.B.H.N. York (Ed.), Life in the Cold, 2000, pp. 431–442.
[38] R.A. Haeusler, T.E. McGraw, D. Accili, Biochemical and cellular properties of insulin receptor signalling, Nat. Rev. Mol. Cell Biol. 19 (1) (2018) 31–44.
[39] R. Ventura-Clapier, A. Garnier, V. Veksler, Transcriptional control of mitochondrial biogenesis: the central role of PGC-1α, Cardiovasc. Res. 79 (2) (2008) 208–217.
[40] M.J. Holness, M.C. Sugden, Regulation of pyruvate dehydrogenase complex activity by reversible phosphorylation, Biochem. Soc. Trans. 31 (Pt 6) (2003) 1143–1151.
[41] V.P. Skulachev, Fatty acid circuit as a physiological mechanism of uncoupling of oxidative phosphorylation, FEBS Lett. 294 (3) (1991) 158–162.
[42] J.R. Davie, Inhibition of histone deacetylase activity by butyrate, J. Nutr. 133 (7 Suppl) (2003) 2485s–2493s.
[43] L.B. Tanner, A.G. Goglia, M.H. Wei, T. Sehgal, L.R. Parsons, J.O. Park, et al., Four key steps control glycolytic flux in mammalian cells, Cell Syst. 7 (1) (2018) 49–62, e48.
[44] D.H. Wasserman, L. Kang, J.E. Ayala, P.T. Fueger, R.S. Lee-Young, The physiological regulation of glucose flux into muscle in vivo, J. Exp. Biol. 214 (Pt 2) (2011) 254–262.
[45] J.P. Schmitz, N.A. van Riel, K. Nicolay, P.A. Hilbers, J.A. Jeneson, Silencing of glycolysis in muscle: experimental observation and numerical analysis, Exp. Physiol. 95 (2) (2010) 380–397.
[46] A.S. Deshmukh, M. Murgia, N. Nagaraj, J.T. Treebak, J. Cox, M. Mann, Deep proteomics of mouse skeletal muscle enables quantitation of protein isoforms, metabolic pathways, and transcription factors, Mol. Cell. Proteomics 14 (4) (2015) 841–853.
[47] P. Fisel, E. Schaeffeler, M. Schwab, Clinical and functional relevance of the monocarboxylate transporter family in disease pathophysiology and drug therapy, Clin. Transl. Sci. 11 (4) (2018) 352–364.
[48] D. Rakus, A. Gizak, A. Deshmukh, J.R. Wisniewski, Absolute quantitative profiling of the key metabolic pathways in slow and fast skeletal muscle, J. Proteome Res. 14 (3) (2015) 1400–1411.
[49] M.E. Walsh, A. Bhattacharya, K. Sataranatarajan, R. Qaisar, L. Sloane, M. M. Rahman, et al., The histone deacetylase inhibitor butyrate improves metabolism and reduces muscle atrophy during aging, Aging Cell 14 (6) (2015) 957–970.
[50] K. Bouter, G.J. Bakker, E. Levin, A.V. Hartstra, R.S. Kootte, S.D. Udayappan, et al., Differential metabolic effects of oral butyrate treatment in lean versus metabolic syndrome subjects, Clin. Transl. Gastroenterol. 9 (5) (2018) 155.
[51] R.A. DeFronzo, D. Tripathy, Skeletal muscle insulin resistance is the primary defect in type 2 diabetes, Diabetes Care 32 (Suppl 2) (2009) S157–S163.
[52] H.W. Tan, A.Y. Sim, S.L. Huang, Y. Leng, Y.C. Long, HC toxin (a HDAC inhibitor) enhances IRS1-akt signalling and metabolism in mouse myotubes, J. Mol. Endocrinol. 55 (3) (2015) 197–207.
[53] C. Sun, J. Zhou, Trichostatin a improves insulin stimulated glucose utilization and insulin signaling transduction through the repression of HDAC2, Biochem. Pharmacol. 76 (1) (2008) 120–127.
[54] O. Klymenko, T. Brecklinghaus, M. Dille, C. Springer, C. de Wendt, D. Altenhofen, et al., Histone deacetylase 5 regulates interleukin 6 secretion and insulin action in skeletal muscle, Mol. Metab. 42 (2020), 101062.
[55] E. Boets, L. Deroover, E. Houben, K. Vermeulen, S.V. Gomand, J.A. Delcour, et al., Quantification of in vivo colonic short chain fatty acid production from inulin, Nutrients 7 (11) (2015) 8916–8929.
[56] J. Frampton, K.G. Murphy, G. Frost, E.S. Chambers, Short-chain fatty acids as potential regulators of skeletal muscle metabolism and function, Nat Metab 2 (9) (2020) 840–848.
[57] M.J. Egorin, Z.M. Yuan, D.L. Sentz, K. Plaisance, J.L. Eiseman, Plasma pharmacokinetics of butyrate after intravenous administration of sodium butyrate or oral administration of tributyrin or sodium butyrate to mice and rats, Cancer Chemother. Pharmacol. 43 (6) (1999) 445–453.
[58] M. Waldecker, T. Kautenburger, H. Daumann, C. Busch, D. Schrenk, Inhibition of histone-deacetylase activity by short-chain fatty acids and some polyphenol metabolites formed in the colon, J. Nutr. Biochem. 19 (9) (2008) 587–593.
[59] A. Galmozzi, N. Mitro, A. Ferrari, E. Gers, F. Gilardi, C. Godio, et al., Inhibition of class I histone deacetylases unveils a mitochondrial signature and enhances oxidative metabolism in skeletal muscle and adipose tissue, Diabetes 62 (3) (2013) 732–742.
[60] P.A. Kakimoto, J.D.C. Serna, V. de Miranda Ramos, A. Zorzano, A.J. Kowaltowski, Increased glycolysis is an early consequence of palmitate lipotoxicity mediated by redox signaling, Redox Biol. 45 (2021), 102026.
[61] D. Sergi, N. Naumovski, L.K. Heilbronn, M. Abeywardena, N. O'Callaghan, L. Lionetti, et al., Mitochondrial (Dys)function and insulin resistance: from

pathophysiological molecular mechanisms to the impact of diet, Front. Physiol. 10 (2019) 532.
[62] C.R. Benton, J.G. Nickerson, J. Lally, X.X. Han, G.P. Holloway, J.F. Glatz, et al., Modest PGC-1alpha overexpression in muscle in vivo is sufficient to increase insulin sensitivity and palmitate oxidation in subsarcolemmal, not intermyofibrillar, mitochondria, J. Biol. Chem. 283 (7) (2008) 4228–4240.
[63] M.P. Mollica, G. Mattace Raso, G. Cavaliere, G. Trinchese, C. De Filippo, S. Aceto, et al., Butyrate regulates liver mitochondrial function, efficiency, and dynamics in insulin-resistant obese mice, Diabetes 66 (5) (2017) 1405–1418.
[64] M. Murgia, N. Nagaraj, A.S. Deshmukh, M. Zeiler, P. Cancellara, I. Moretti, et al., Single muscle fiber proteomics reveals unexpected mitochondrial specialization, EMBO Rep. 16 (3) (2015) 387–395.
[65] A. Goudarzi, The recent insights into the function of ACAT1: a possible anti-cancer therapeutic target, Life Sci. 232 (2019), 116592.
[66] Z. Yang, M. He, J. Austin, J. Pfleger, M. Abdellatif, Histone H3K9 butyrylation is regulated by dietary fat and stress via an acyl-CoA dehydrogenase short chain-dependent mechanism, Mol. Metab. 53 (2021), 101249.